Sun *et al.*
Chinese Journal of Mechanical Engineering (2022) 35:100
https://doi.org/10.1186/s10033-022-00771-8

Chinese Journal of Mechanical Engineering

ORIGINAL ARTICLE

Open Access

Development and Analysis of a New Cylindrical Lithium-Ion Battery Thermal Management System

Yasong Sun[1,2*], Ruihuai Bai[2] and Jing Ma[3]

Abstract

With the development of modern technology and economy, environmental protection and sustainable development have become the focus of global attention. The promotion and development of electric vehicles (EVs) have bright prospects. However, many challenges need to be faced seriously. Under different operating conditions, various safety problems of electric vehicles emerge one after another, especially the hidden danger of battery overheating which threatens the performance of electric vehicles. This paper aims to design and optimize a new indirect liquid cooling system for cylindrical lithium-ion batteries. Various design schemes for different cooling channel structures and cooling liquid inlet directions are proposed, and the corresponding solid-fluid coupling model is established. COMSOL Multiphysics simulation software is adopted to simulate and analyze the cooling systems. An approximate model is constructed using the Kriging method, which is considered to optimize the battery cooling system and improve the optimization results. Sensitivity parameter analysis and the optimization design of system structure are performed through a set of influencing factors in the battery thermal management. The results indicate that the method used in this paper can effectively reduce the maximum core temperature and balance the temperature differences of the battery pack. Compared with the original design, the optimized design, which is based on the non-dominated sorting genetic algorithm (NSGA-II), has an excellent ability in the optimized thermal management system to dissipate thermal energy and keep the overall cooling uniformity of the battery and thermal management system. Furthermore, the optimized system can also prevent thermal runaway propagation under thermal abuse conditions. In summary, this research can provide some practical suggestions and ideas for the engineering and production applications and structural optimization design carried by electric vehicles.

Keywords: Cooling system, Electric vehicle, Kriging approximation, Numerical simulation

1 Introduction

With the increasingly severe environmental pollution, the concept of environmental protection is constantly deepening on a global scale. To reduce urban carbon emissions and improve air quality, the promotion and development of electric vehicles are of great significance. As the power source of electric vehicles, lithium batteries have the advantages of high specific energy and long cycle life. However, due to the characteristics of being sensitive to temperature changes [1], lots of battery thermal runaway problems occur under extreme ambient temperatures. Moreover, battery thermal management (BTM) is essential to solving a series of issues, for example, battery heat dissipation in electric vehicles [2].

At present, the BTM system in electric vehicles is divided into three categories: air cooling, liquid cooling, and phase change cooling [3]. The air-cooling type has some great abilities of more choices of pipeline layout, high-cost performance, and lower maintenance

*Correspondence: yssun@nwpu.edu.cn

[1] School of Power and Energy, Northwestern Polytechnical University, Xi'an 710072, China
Full list of author information is available at the end of the article

costs [4]. However, due to the limited heat dissipation capacity of the air-cooled BTM system, poor cooling uniformity, and low NVH (noise, vibration, and roughness) [5], its application has been limited. The Phase change material (PCM) BTM system is a reliable cooling technology with the advantages of reliability and safety [6]. However, the PCM-based BTM system is still in the laboratory research and exploration stage [7]. PCM-based BTM systems mainly include pure PCM, composite PCM, and hybrid PCM. Chen et al. [8] review the advantages and disadvantages of PCM-based BTM systems. They got conclusions through research that the thermal conductivity in most of the single PCM-based BTM systems is very low, which would result in a significant amount of thermal energy accumulation in the battery system in an extreme temperature working environment. To improve the thermal conductivity and strengthen the material, carbon materials and metals are optionally added in phase change materials. The hybrid PCM BTM system has better effects on improving the uniformity of battery temperature distribution and reducing battery temperature rise. In addition, the heat dissipation problem of the battery module is studied based on the orthogonal experimental design in the literature [9]. The application of graphene in energy storage technology and thermal energy transfer have also been studied. Due to the superior cooling performance and more flexible pipeline layout, the liquid cooling method has been widely applied in electric vehicles, such as Tesla Model S and Chevrolet Volt. The thermal management of a cylindrical battery with double profiles is more complicated than a six-sided cylindrical unit. As the increase of power battery density, the thermal energy generated in the cylindrical battery has also increased. The liquid-cooled BTM system has become an essential and applicable solution for lithium battery cooling technology in electric vehicles [10]. Tesla designed a bellows belt with a double inlet and outlet to control the heat distribution of the 18650 battery [10]. Zhao et al. [11] developed and researched a cooling jacket with microchannels to control the temperature distribution of the 18650 battery. They also investigated the effects of channel number, channel size and fluid flow on the temperature profiles of the battery. Rao et al. [12] used a heat-conducting device with a liquid channel to cool the cylindrical battery. This device could effectively dissipate the heat generated by the battery. Sheng et al. [13] developed a battery liquid cooling jacket that could satisfy the requirements of the cooling effect for the 21700 lithium-ion battery. They numerically investigated the influence of fluid flow, channel size and cooling medium on the thermal characteristics of the battery. These numerical results had been validated by the experimental results. Tete et al. [14] devised a cooling solution halfway between direct and indirect cooling, inserting the battery pack into a cylindrical housing and circulating liquid cooling medium around the battery. It can be concluded from the above researches that the combinations of the cooling sleeve and liquid cooling are effective schemes for the geometrical structure and thermal characteristics of the cylindrical batteries. However, relevant researches are still insufficient at present, meanwhile, there is a lack of relevant researches on electrochemical models that can simulate the charging and discharging process of real batteries through combining thermal management system, as well as the researches on the specific effects of various geometric parameters of cooling jackets using scientific optimization methods.

In order to promote the physics-based models in real-time applications, Deng et al. [15] applied a series of model reduction methods in this study to obtain a reduced order model (ROM) of all-solid-state batteries. Compared with the original PDE-based model, the voltage error of the proposed ROM is smaller. To simplify the evaluation and simulation of the battery performance, Hallaj et al. [16] developed a one-dimensional mathematical model to simulate the internal temperature curve of cylindrical lithium-ion batteries, and analyzed the effect of simplified batteries. As that the BTM system has a high cooling rate, the sensitivity of the electrochemical reaction of the cylindrical battery to the temperature gradient can be ignored. Al-Zareer et al. [17] proposed a one-dimensional model to simulate the electrochemical reaction, and a three-dimensional model to simulate the thermal distribution of the battery. Since the purpose of the BTM system is to stabilize the temperature in the proper range, the electrochemical reactions of the battery are used to set up the model for predicting the amount of heat generated accurately.

Aiming to solve the problem of the temperature differences and the uneven distribution of 21700 cylindrical batteries, a new columnar liquid-cooled BTM system cooling sleeve is proposed in this paper. Compared with the traditional cooling sleeve, the batteries are scattered inside the cooling sleeve, and the number of cooling channels is larger. In the process of the study, it is found that the average temperature of the battery core is the highest. Therefore, the diameter of the cooling channel increases in the center position nearest to the adjacent battery cell can improve the heat dissipation effect of the battery. The electrochemical model, which can simulate the actual battery discharge process, is used to simulate the numerical simulation. Aiming at the numerical simulation of BTM cooling system, the cooling performance of cooling jacket in the flow

direction of the cooling medium and the size of the cooling channel are analyzed. Thus, the BTM system is optimized by approximate model and multi-objective optimization.

2 Physical and Numerical Models of BTM System

2.1 Physical Model of BTM System

The integrated battery pack BTM system [18] is shown in Figure 1. The integrated battery pack comprises 21700 batteries in parallel and embedded in the aluminum cooling sleeve. The liquid cooling holes are distributed between the batteries. The cooling medium (water- ethylene glycol) flows through the cooling channel to cool the cooling sleeve, taking away the thermal energy generated by the battery. The physical model of the battery pack can be simplified as the right hand of Figure 1 using the symmetries.

As shown in Figure 1, the battery model is established by the actual parameters of the 21700 battery, and the geometric parameters of the battery model are shown in Table 1. The height and the outer diameter are 70 mm and 10.72 mm, respectively. The core diameter and the shell thickness are 3.2 mm and 0.22 mm, respectively.

In this paper, the COMSOL Multiphysics software [19] is used to model, simulate and analyze the BTM system, which is a comprehensive multi-platform finite element solver that can simulate electronic, physical, and mechanical systems.

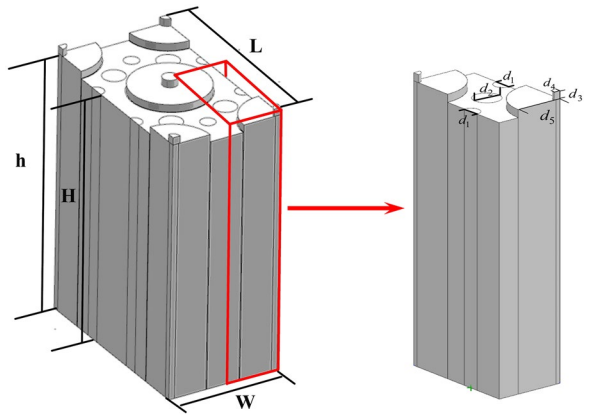

Figure 1 The battery pack and simplified model

2.2 Numerical Model of BTM System

In order to study the cooling performance of the BTM system and obtain the temperature distributions in the battery, two independent models are developed to simulate the integrated battery pack and BTM system. One model is a one-dimensional electrochemical model that is constructed to the electrochemical reaction in batteries and the temperature variations under different working conditions. The other model is a three-dimensional thermal energy transfer model consisting of the battery pack and BTM system.

The electrochemical reactions in the spiral direction can be ignored, and the electrochemical performance of the cylindrical battery can be evaluated by a one-dimensional electrochemical model [20]. The simulation domain and boundary conditions of this model are depicted in Figure 2.

The electrochemical and thermal energy transfer models are concatenated through the generated heat source and the average temperature. These two joint models determine the cooling performance of the proposed BTM system. The average temperature of the battery which is used in the one-dimensional electrochemical model, can be obtained from the thermal energy transfer model. In addition, the electrochemical model feeds the average heat source into the heat transfer model through simulation calculation. Then the heat and temperature distributions of the battery are simulated and calculated using the heat transfer model.

2.2.1 Three-Dimensional Thermal Energy Transfer Model

The computational domain of the three-dimensional thermal energy transfer model is shown in Figure 3a.

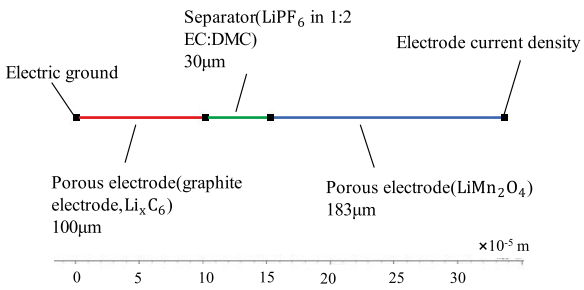

Figure 2 The computational domain of the electrochemical model and boundary condition

Table 1 Battery model geometric parameters mm

Symbol	d_1	d_2	d_3	d_4	d_5	H	h	L	W
Value	4	6	3.2	3.2	10.72	68	70	30.53	52.88

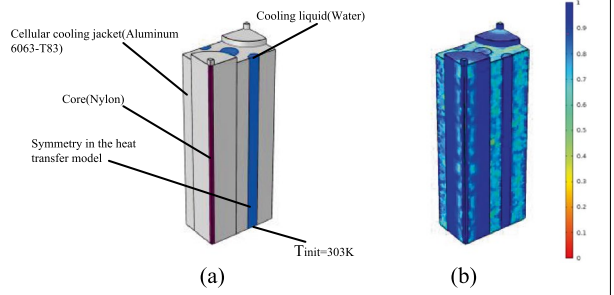

Figure 3 **a** The computational domain of three-dimensional thermal energy transfer model, **b** the quality of mesh

Two quarters of the battery and cooling channels in the domain are embedded in the aluminum cooling sleeve. The mesh quality selected for the three-dimensional thermal energy transfer model is shown in Figure 3b. The control equations can be expressed by the energy balance equation and the coolant's mass, momentum, and energy conservation equations. The conservation equation of battery energy rate can be expressed as:

$$\frac{\partial}{\partial t}\left(\rho_b c_{p,b} T_b\right) = \nabla \cdot \left(k_b \nabla T_b\right) + \dot{Q}_{gen}, \tag{1}$$

where ρ_b,$c_{p,b}$,k_b are the battery density, specific heat capacity and thermal conductivity of battery material, respectively. ∇T_b represents the temperature distribution of the battery in a process, $\dot{Q}_{gen}$ is the thermal energy generated in the battery.

The mass, momentum and energy balance equation of the coolant are:

$$\frac{\partial \rho_b}{\partial t} + \nabla \cdot \left(\rho_P \vec{v}\right) = 0, \tag{2}$$

$$\frac{\partial}{\partial t}\left(\rho_P \vec{v}\right) + \nabla \cdot \left(\rho_P \vec{v}\vec{v}\right) = -\nabla P + \rho g, \tag{3}$$

$$\frac{\partial}{\partial t}\left(\rho_b c_{p,b} T_b\right) + \nabla \cdot \left(\rho_b c_{p,b} \vec{v} T_p\right) = \nabla \cdot \left(k_p \nabla T_p\right), \tag{4}$$

where the subscript b is the cooling medium, P is the pressure, g is the gravity acceleration, $\vec{v}$ is the velocity vector of coolant.

The volume heating rate of the electrochemical model is obtained and applied to the active material part of the battery model. Compared with the heat production rate from the BTM system, the heat production rate at the battery connector can be ignored. Thus, the insulation boundary condition is used. The battery pack consists of several single cells, which are lithium-ion prismatic cells. The thermal conductivity in the thermal energy transfer model is anisotropic, and the thermal conductivity along the direction of the battery plate (cylinder length direction) is higher than that in the normal (radial) direction of the battery plate.

In the radial direction, the thermal conductivity k_r is calculated by the following formula [21]:

$$k_r = \frac{\sum L_i}{\sum \left(L_i / k_i\right)}, \tag{5}$$

where L_i is the thickness of the ith layer of one single battery, and k_i represents the thermal conductivity of the material.

The thermal conductivity in the length direction of cylinder is:

$$k_z = \frac{\sum \left(L_i k_i\right)}{\sum L_i}. \tag{6}$$

Similarly, $c_{p,b}$ and ρ_b the heat capacity and the density of battery material.

$$c_{p,b} = \frac{\sum \left(L_i c_{p,i}\right)}{\sum L_i}, \tag{7}$$

$$\rho_b = \frac{\sum \left(L_i \rho_i\right)}{\sum L_i}. \tag{8}$$

2.2.2 One-Dimensional Electrochemical Model

The one-dimensional electrochemical model was established by Doyle et al. [22] and Fuller et al. [23]. The constant current charge and discharge of the lithium anode battery are modelled by using the concentrated solution theory. The equilibrium voltage changes of negative and positive electrode materials are based on the experimental results of Doyle et al. [20]. Fuller et al. [23] further studied the double lithium-ion insertion battery and optimized the active battery material.

The two porous electrodes sandwiched in the third layer of non-aqueous electrolyte are the main structure of the battery. The electrode has a porous structure, and the diaphragm is a multi-component system of plastic composed of five polymers, two kinds of liquids, one cation, and one anion. The change of the salt concentration in the electrode solution can be described as follows:

$$\frac{\partial b_s}{\partial t} = \frac{1}{\varepsilon}\left[\nabla \cdot \left(D_s \nabla b_s\right) + \left(a j_n + a j_n t_+^0\right) - \frac{i_2 \cdot \nabla t_+^0}{F}\right], \tag{9}$$

where b_s is the salt concentration in the electrode, D_s represents the diffusion coefficient of the electrode, a is the specific interface part, t is time, i_2 represents the current density at the surface of the liquid phase, and j_n represents lithium-ion pore wall flux. The subscript "+" in the

formula represents positive and "−" represents negative, correspondingly. The relationship between the lithium-ion surface current density and the lithium-ion pore wall flux is:

$$j_n(aF) = \nabla \cdot i_2, \tag{10}$$

where the surface density of the liquid phase i_2 represents the function of the electrolyte concentration, time, the conductivity, the absolute temperature, the activity coefficient, and electrode solution-phase potential. It can be expressed as:

$$i_2 = -k\nabla\phi_2 + \left(\frac{2kRT}{F} + \frac{2kRT}{F}\frac{\partial \ln f_{\pm}}{\partial \ln b_S}\right)\left(1 - t_+^0\right)\nabla \ln b_S, \tag{11}$$

where, F represents the Faraday constant, 96587 C/mol and R represents the general gas constant, $8.314\mathrm{J}/(\mathrm{mol}\cdot\mathrm{K})$. The solid phase current density (i_1) is the function of the solid-electrode potential and the electronic conductivity of solid-phase mixture,

$$i_1 = -\sigma\nabla\phi_1. \tag{12}$$

The concentration of lithium element in the solid matrix of the battery electrode can be expressed as:

$$\frac{\partial b_{Li}}{\partial t} = D_{Li}\left[\frac{2}{r}\frac{\partial b_{Li}}{\partial r} + \frac{\partial^2 b_{Li}}{\partial r^2}\right], \tag{13}$$

where D_{Li} represents the diffusion coefficient of lithium-ion in solid electrode phase, r is the radial direction of battery.

The following formula is the Butler-Volmer kinetic equation, connecting the solid and liquid phases,

$$\left(\frac{j_n}{H}\right) + (b_S)^{0.5}(b_i - b_{Li})^{0.5}(b_{Li})^{0.5}\exp\left[-\frac{F}{2RT}(\eta - V_{OC})\right] = (b_S)^{0.5}(b_i - b_{Li})^{0.5}(b_{Li})^{0.5}\exp\left[\frac{F}{2RT}(\eta - V_{OC})\right], \tag{14}$$

$$\frac{\partial b_S}{\partial r} = -j_n/D_{Li}, \tag{15}$$

H represents the result of multiplying positive and negative chemical reaction constants, b_i represents the salt concentration of the ith layer, b_{Li} represents the solid lithium concentration, η is the battery electrode potential, V_{oc} represents the open-circuit voltage. The battery electrode potential is expressed by the following formula:

$$\eta = \phi_1 - \phi_2. \tag{16}$$

In this paper, the lithium battery cathode material is graphite (Li_xC_6), the anode material is lithium manganate ($LiMn_2O_4$). The plasticized electrolyte is a multi-component $LiPF_6$ strip in a non-aqueous liquid mixture of the ethyl carbonate and the dimethyl carbonate solvents. The changes in electrolyte ionic conductivity were obtained from experimental results presented by Doyle et al. [20] and numerical results by Al-Zareer et al. [24]. Figure 4 shows the ionic conductivity change of 1:2 ethyl carbonate: dimethyl carbonate solvent.

The electrochemical model positive electrode material is $LiMn_2O_4$, the electrical conductivity is 3.8 S/m, the maximum charge state of the electrode is 0.995, and the minimum charge state is 0.175. The temperature derivative of electrode equilibrium potential changes with the measured state of charge (SOC), and the electrode equilibrium potential changes with the positive SOC are shown in Figures 5 and 6. By comparing the numerical simulation results with Al-Zareer et al. [24], it can be concluded that the electrochemical model in this paper is precise in simulating the change of the positive electrode equilibrium potential.

As shown in Figure 7, the curves of the potential and the battery capacity of a one-dimensional electrochemical model at different rates are compared with the study of Doyle et al. [20]. The comparison results show that the model can accurately predict the electrochemical behaviour of lithium-ion batteries.

Figure 8 shows the change of the negative open electrode potential with the charge state distribution in the electrochemical model, which is verified by comparison with the experimental results of Doyle et al. [20].

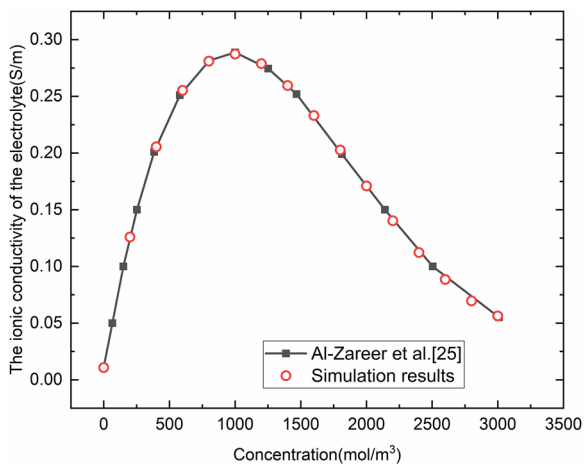

Figure 4 The variation of the ionic conductivity of the electrolyte with the slat concentration for 1:2 ethylene carbonate: dimethyl carbonate solvent

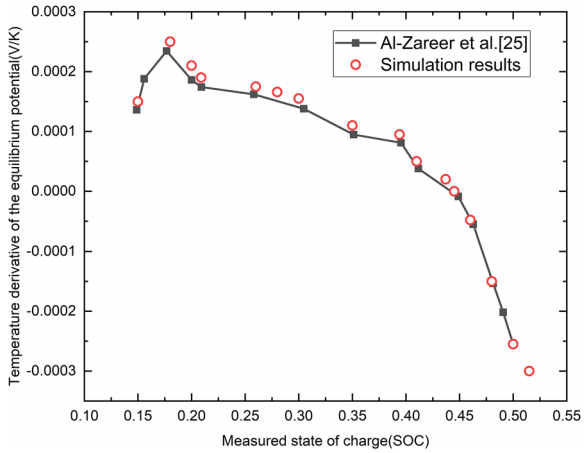

Figure 5 The variation of the temperature derivative of the equilibrium potential of the electrode with the SOC of the positive electrode

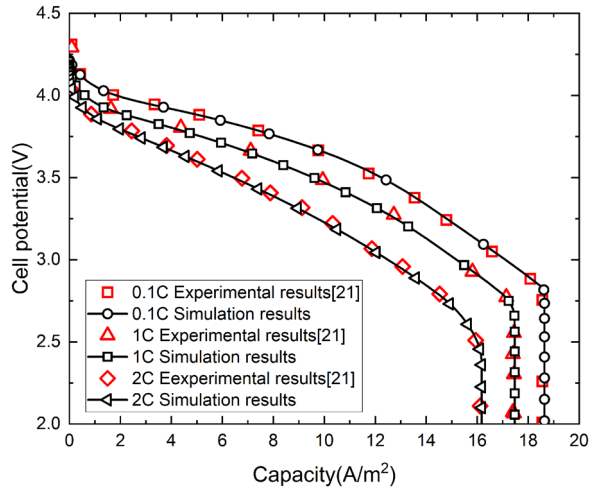

Figure 7 Comparisons of a one-dimensional electrochemical model at different rates with the results of Doyle et al [20]

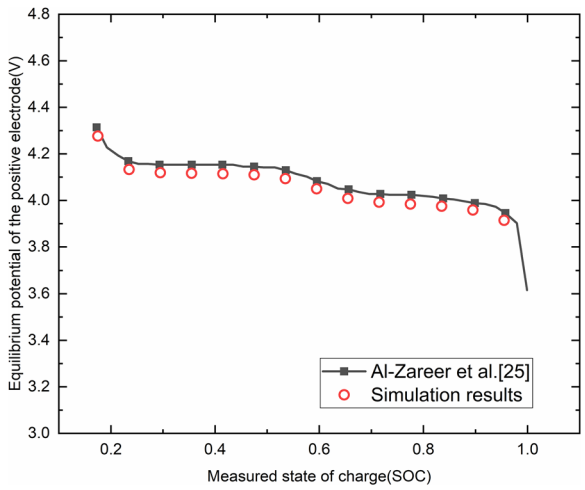

Figure 6 The variation of the equilibrium potential of the positive electrode with the measured state of charge

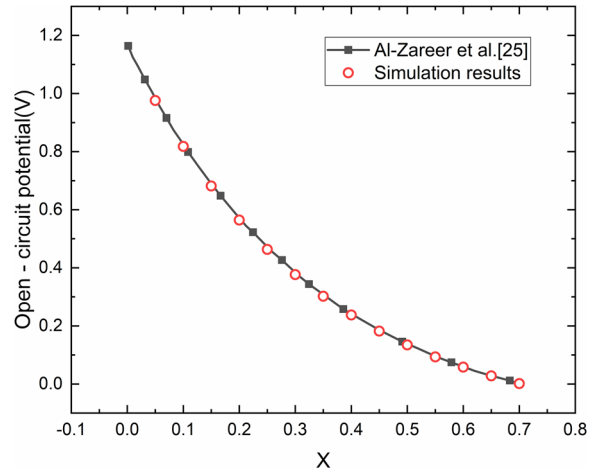

Figure 8 The negative open circuit potential varies with the charge state distribution

3 Effects of the Flow Direction and the Cooling Channel Sizes

In this section, the effects of the flow direction of the cooling medium and the structure size of the cooling channel on the cooling performance of the BTM system are analyzed. The initial temperature and the ambient temperature are both 303 K, and the temperature variations of the battery core shaft are monitored in the simulation process.

3.1 Effect of the Flow Direction

The influence of the fluid flow direction on the cooling performance of the initially designed BTM system is analyzed in this section. As shown in Figure 9, according to the different positions of the inlet and outlet of the cooling channel, a total of three different layouts of the cooling channel are designed, in which "⊠" and "⊙" denote the inflow or outflow of fluid along the vertical direction of the paper surface, respectively.

Figure 9 shows the variation curves of the average temperature of the battery core axis in the case of each channel layout when the battery module is discharged at 4 C at the inlet velocity of 0.795×10^{-2} m·s^{-1} in each cooling channel.

What can be noticed from Figure 10 is that the average temperature of the central axis increases with time.

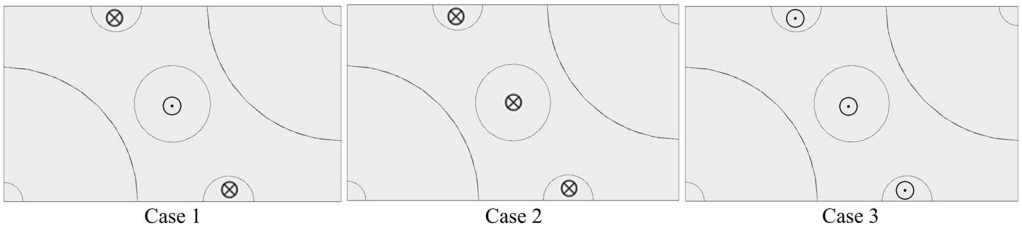

Figure 9 The effect of flow direction

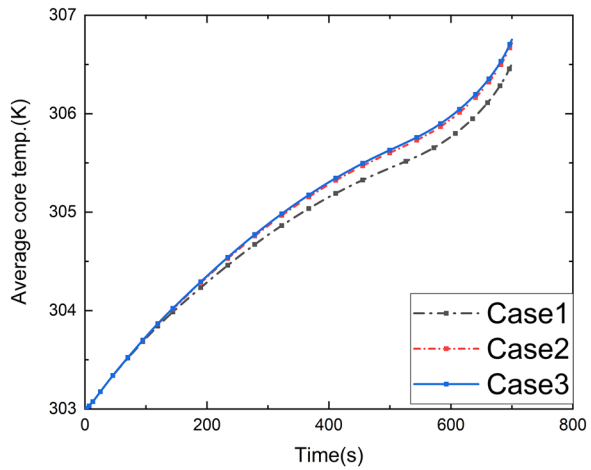

Figure 10 The average temperature variation along battery core axis

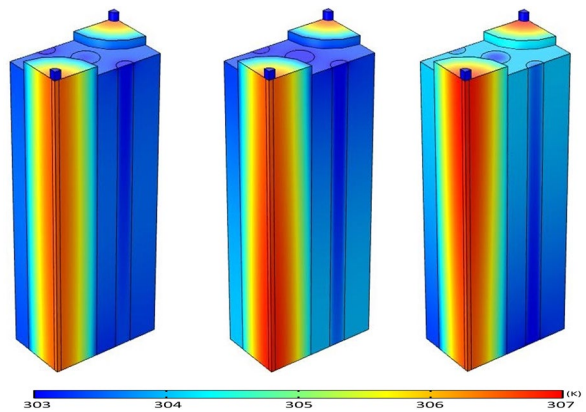

Figure 11 Thermal profiles of the battery and the surface temperature distribution of BTM system

The reason is that the growth trend of "fast–slow–fast" of temperature variation is mainly attributed to the battery internal resistance [6]. In Figure 10, the temperature rise of all the cases is within 4 K, the average temperature rise of case 1 is the lowest, and the difference between case 2 and case 3 is within 0.2 K.

Figure 11 shows the thermal profiles of the battery and the temperature distributions on the surface of the BTM system at 700 s. What can be seen is that the battery temperature gradually increases along the axial direction and reaches the maximum temperature at the core axis of the battery. In Case 1, for staggered cooling channel layout, the average temperature of the battery is low, and the temperature distribution uniformity is good.

Consequently, the staggered flow channel arrangement has advantages in controlling the heat production and the thermal uniformity of the battery. The cooling channel arrangement of case 1 has better cooling performance for this BTM system.

3.2 Effect of the Cooling Channel Size

In this section, three different cooling channel diameters are initially designed, and the influences of different

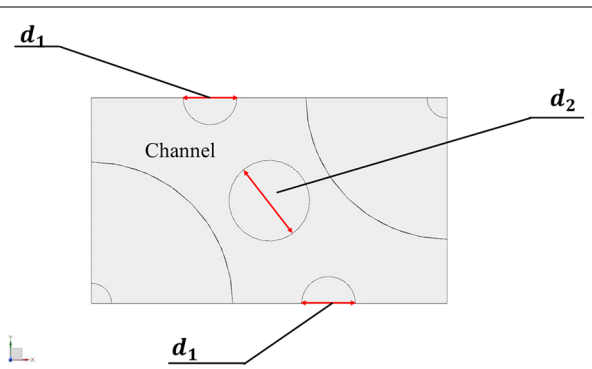

Figure 12 The physical model of a cooling channel

cooling channel sizes on heat distribution are preliminary studied. Figure 12 shows the cooling channel overlooking the cooling sleeve, where $d_1 - d_3$ denotes the diameter of three adjacent cooling channels.

In the case of the battery module discharges at 4 C rate, the inlet flow rate is $0.795 \times 10^{-2}\mathrm{m} \cdot \mathrm{s}^{-1}$, the staggering flow arrangement of the cooling channel, the result of the cooling channel sizes on the battery temperatures at the axis center is depicted in Figure 13. Figure 14 shows

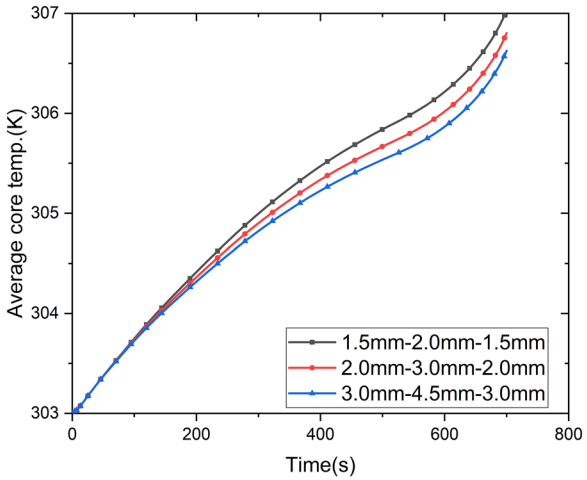

Figure 13 The result of the cooling channel size on the temperature curves of battery

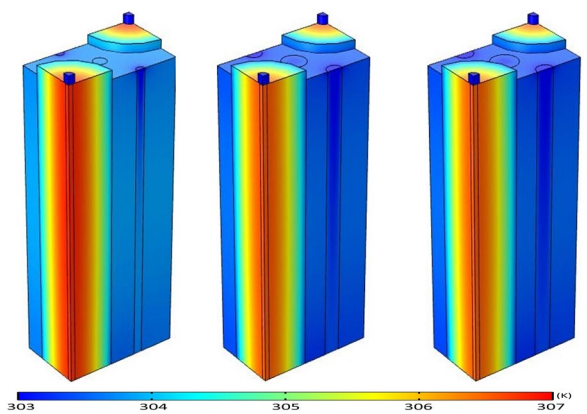

Figure 14 Thermal profile of battery modules with different cooling channel sizes and surface temperature distributions of BTM system

the thermal profiles of the battery module and the surface temperature distributions of the BTM system at each cooling channel size at 700 s. When the diameter of the cooling channel d_1 and d_3 increase from 1.5 mm to 3.0 mm, d_2 increases from 2.0 mm to 4.5 mm, the size of the cooling channel has the most significant impact on the temperature rise of the core axis for 21700 battery, and the maximum temperature difference between all design sizes is within 0.5 K.

From the above results, expanding the cooling channel diameter is good for enhancing the cooling effect of the BTM system to a certain extent. The following section focuses on studying the influences of the cooling channel diameter (d_1, d_2), the cooling jacket height (h), and the inlet velocity (v_0) on heat dissipation of the BTM system, aiming to obtain the best design results within the acceptable parameter range.

4 Approximate Model and Multi-Objective Optimization of BTM System

The approximate model and multi-objective optimization are established in this section. Also, the influence of geometric parameters of a cooling sleeve in the thermal management system is analyzed. All numerical calculations involved are performed in COMSOL. Firstly, the geometric design of the BTM system is completed, and the numerical calculations have obtained the results under the initial conditions. Secondly, to obtain the corresponding output targets through the generated sample points, 30 sample points are considered to be obtained by the DOE method. The Kriging method is used to construct the approximate model, and the multi-direction multi-objective optimization scheme is considered, including the design parameters, the objective parameters, and constraints. The NSGA-II method [25, 26] is used to operate the optimization model, and the Pareto surface is obtained considering the average cell temperature (ACT) and the maximum temperature difference (MTD). Finally, the optimal design is selected by comparing the performance difference between the optimal design and the initial unoptimized design.

4.1 Approximate Model

The Kriging method is constructed to establish a high-dimensional approximate model. It can effectively improve the numerical simulation calculation cost while obtaining numerical calculation accuracy. Kriging is an approximate model method that is generally used to approximate a set of input and output variables.

Figure 15 shows the flowchart of the establishment of the Kriging model. The DoE sampling strategy chooses a series of sampling points to perform numerical simulation and takes the numeral calculation on sampling points. Constructing the basis function and inputting the calculation results of the above sample points into the Kriging model, the fitting curve of the first-order term and the fitting surface of the second-order term are obtained. Finally, the accuracy of the Kriging model is tested.

4.2 Evaluation of the Approximate Model

The structural stability and practicality of the proposed BTM system need to be considered when determining the range of influencing parameters, which are shown in Table 2.

The established approximate model is based on the Kriging method [27]. The research uses the numerical

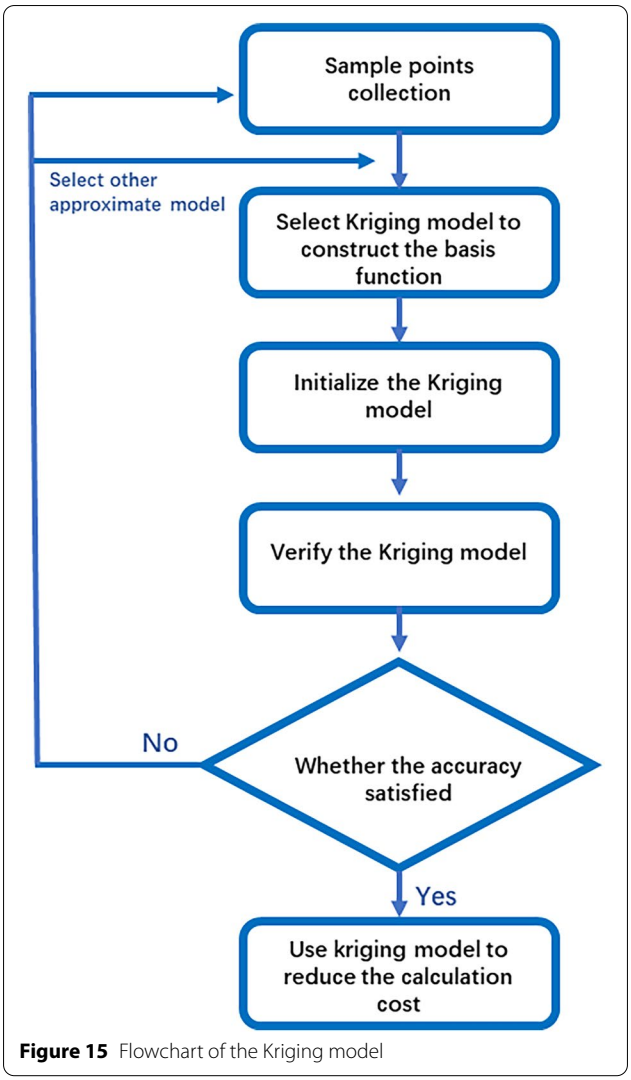

Figure 15 Flowchart of the Kriging model

Table 2 The design variables and corresponding variation range

Variables	Unit	Lower limit	Upper limit	Original value
d_1	mm	2.2	6.8	1.5
d_2	mm	3.0	6.6	2
h	mm	65.0	70.0	68
v_0	m/s	0.001	0.0725	0.005

Table 3 Accuracy of Kriging models

Output	RMSE	*R*-square
MTD	0.09788	0.91318
ACT	0.11960	0.90002

simulation calculation when the battery pack is discharged at a 4 C rate. This setting ensures that the proposed BTM system meets the battery thermal energy dissipation requirements. In order to verify the approximate model of the BTM system, eight groups of sample points related to four factors in sequence are selected and calculated. R-square (R^2) and root mean square ($RMSE$) are introduced to evaluate the fit accuracy. The calculation formula for the accuracy of the constructed approximate model is expressed as follows:

$$R^2 = 1 - \frac{\sum_{i=1}^{m}\left[f\left(x^i\right) - \hat{f}\left(x^i\right)\right]^2}{\sum_{i=1}^{m}\left[f\left(x^i\right) - \bar{f}\right]^2}, \tag{17}$$

$$RMSE = \sqrt{\frac{\sum_{i=1}^{m}\left[f\left(x^i\right) - \hat{f}\left(x^i\right)\right]^2}{m}}. \tag{18}$$

As listed in Table 3, the accuracy of the Kriging model is good.

4.3 Multi-Objective Design Optimization Scheme

The liquid cooling BTM system uses multi-objective design optimization (MODO) which there are two optimization objectives, namely the minimization of MTD and ACT. On the premise of satisfying the requirements of battery thermal energy and reducing the risk of heat runaway transmission, improving the performance of the battery thermal management system, the average core temperature and the maximum temperature difference of the battery are the optimization ranges. Four highly sensitive influencing factors are selected as the input parameters of the optimized design, including the cooling channel diameter (d_1, d_2), the height of the cooling jacket (h), and the cooling channel inlet velocity (v_0). The constraints of the proposed optimization model can be expressed in the following form:

$$\begin{cases} \text{variables } \vec{x} = [d_1, d_2, h, v_0], \\ \text{MTD} = f_{\text{MTD}}(\vec{x}), \\ \text{ARC} = f_{\text{ARC}}(\vec{x}), \\ \text{objectives find } \vec{x} = [d_1, d_2, h, v_0], \\ \min\ \text{MTD}, \\ \min\ \text{ACT}, \\ \text{constraints } 2.2 \le d_1 \le 6.8, \\ 3.0 \le d_2 \le 6.6, \\ 65.0 \le h \le 70.0, \\ 0.001 \le v_0 \le 0.0725. \end{cases} \tag{19}$$

5 Results and Discussions

5.1 Average Core Temperature (ACT)

ACT is the average temperature of the battery core when the battery reaches the cut-off voltage during the discharge process. Therefore, ACT can be used to reflect the cooling efficiency of the BTM system. As shown in Figure 16(a)–(d), a single variable affects the average core temperature. Figure 17(a)–(c) show the influence of two parameters on the average core temperature.

As shown in Figures 16(a), (b), and 17(a), ACT decreases with the increase of the cooling channel diameter. Meanwhile, as d_1 and d_2 increase, the downward trend of ACT gradually decreases. Figures 16(c) and 17(b) show that increasing the height of the cooling jacket can reduce the ACT, but the trend is slight. According to Figures 16(d) and 17(c), expanding the inlet coolant flow velocity lowers ACT. Therefore, to improve the thermal energy dissipation efficiency, increasing the diameter of the cooling channel and the flow velocity are good choices.

5.2 Maximum Temperature Difference (MTD)

MTD is the parameter that represents the temperature uniformity of the battery surface. In contrast to ACT, the influence of geometrical parameters of cooling passage on MTD is not significant. Figures 18(c) and 19(b) show that MTD decreases with the increase of the height of the cooling jacket. Figures 18(d) and 19(c) show that MTD increases first and then decreases with the increase of coolant inlet velocity. Therefore, specific inlet velocity is selected to enhance the cooling efficiency of the BTM system.

It can be concluded that the expansion of the diameter of the cooling channel (d_1, d_2) significantly reduces ACT; while the increasing of the cooling jacket height reduces MTD. The diameter of channel 2(d_2) almost has no effect

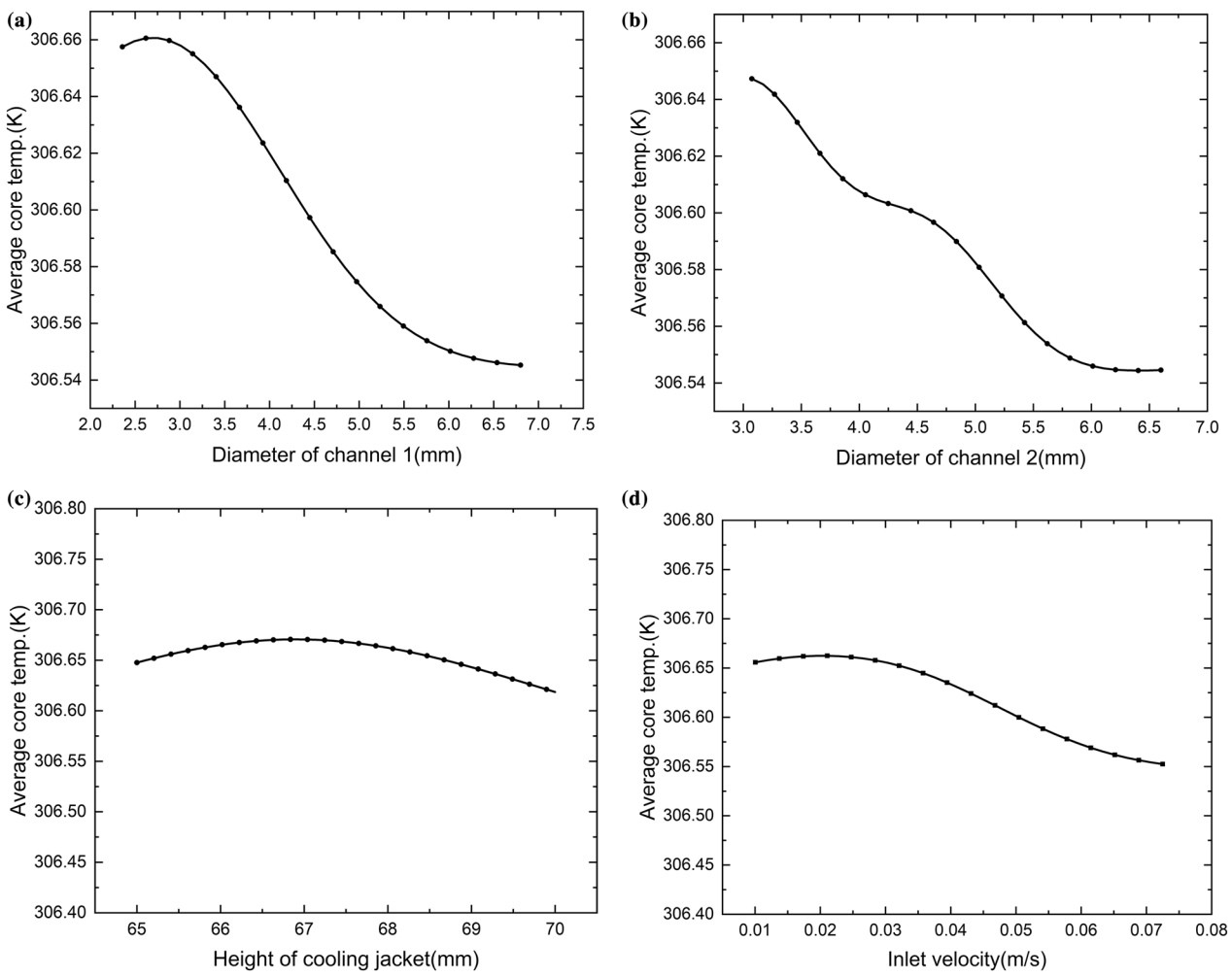

Figure 16 The prediction of the average core temperature of BTM system (first-order terms)

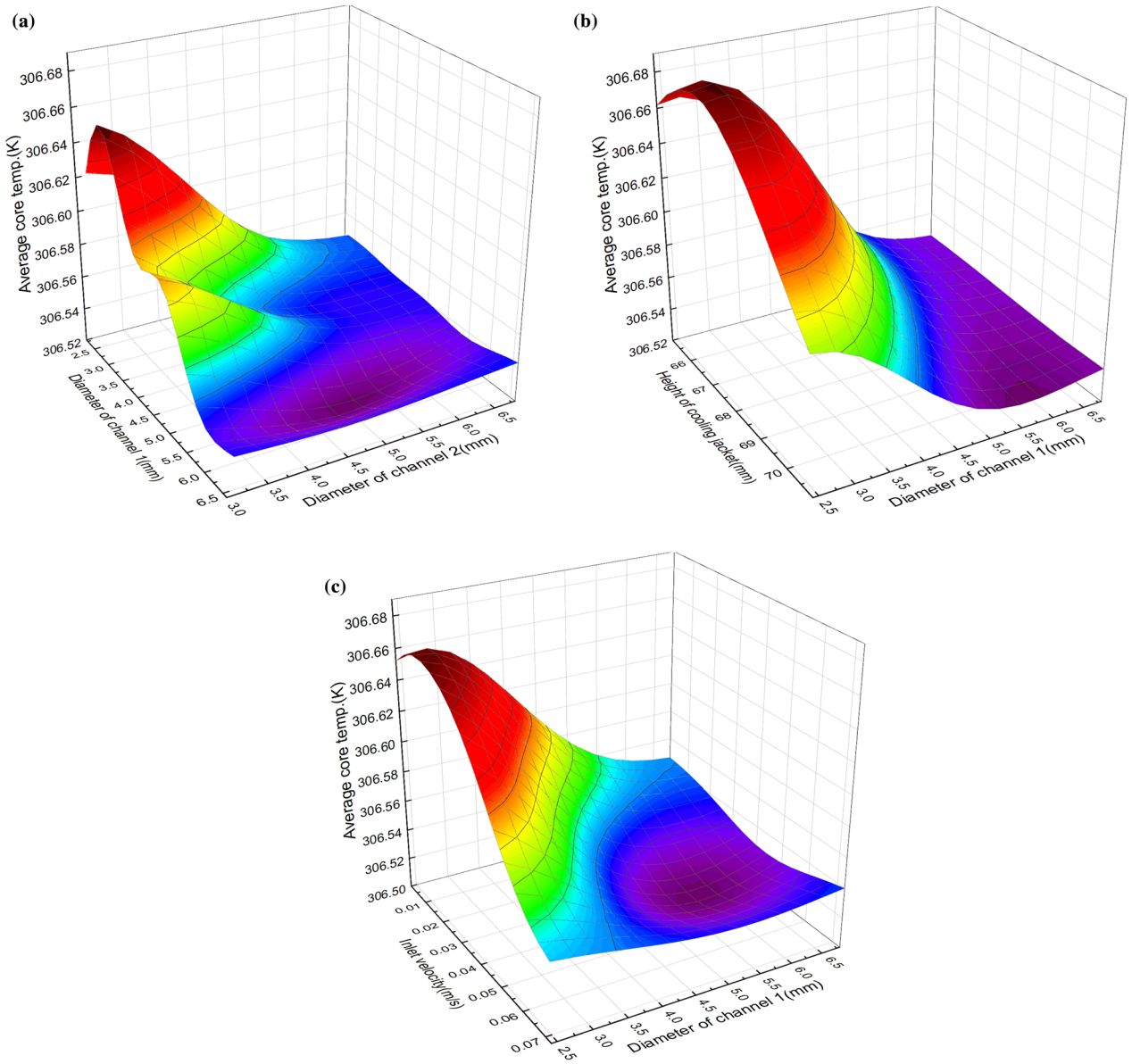

Figure 17 The prediction of the average core temperature of the BTM system (second-order terms)

on MTD. Thus, when the cooling channel diameter is large, the inlet coolant flow rate should be increased to improve the overall performance of the system.

5.3 Multi-Objective Optimization Result

When the MOPSO framework is established, the NSGA-II algorithm is used to construct the optimization work. For the setting of NSGA-II, the population size, the crossover probability, and the number of generations are 12, 0.9 and 20, respectively. The Pareto solution set based on the MOPSO algorithm is shown in Figure 20, which Pareto solution set Front arc AB is Pareto optimal solution set.

According to the result of the Pareto solution set and the Pareto optimal solution set, the inability to achieve good heat dissipation as a whole may result in significant battery temperature differences., Within the average core temperature range, the maximum temperature difference stabilizes in the range of 306.45 K to 306.55 K. However, when the average core temperature is below 306.45 K, the temperature difference increases sharply. Table 4 shows the parameter values of the optimized and the original design. When the battery discharges at 4 C discharge

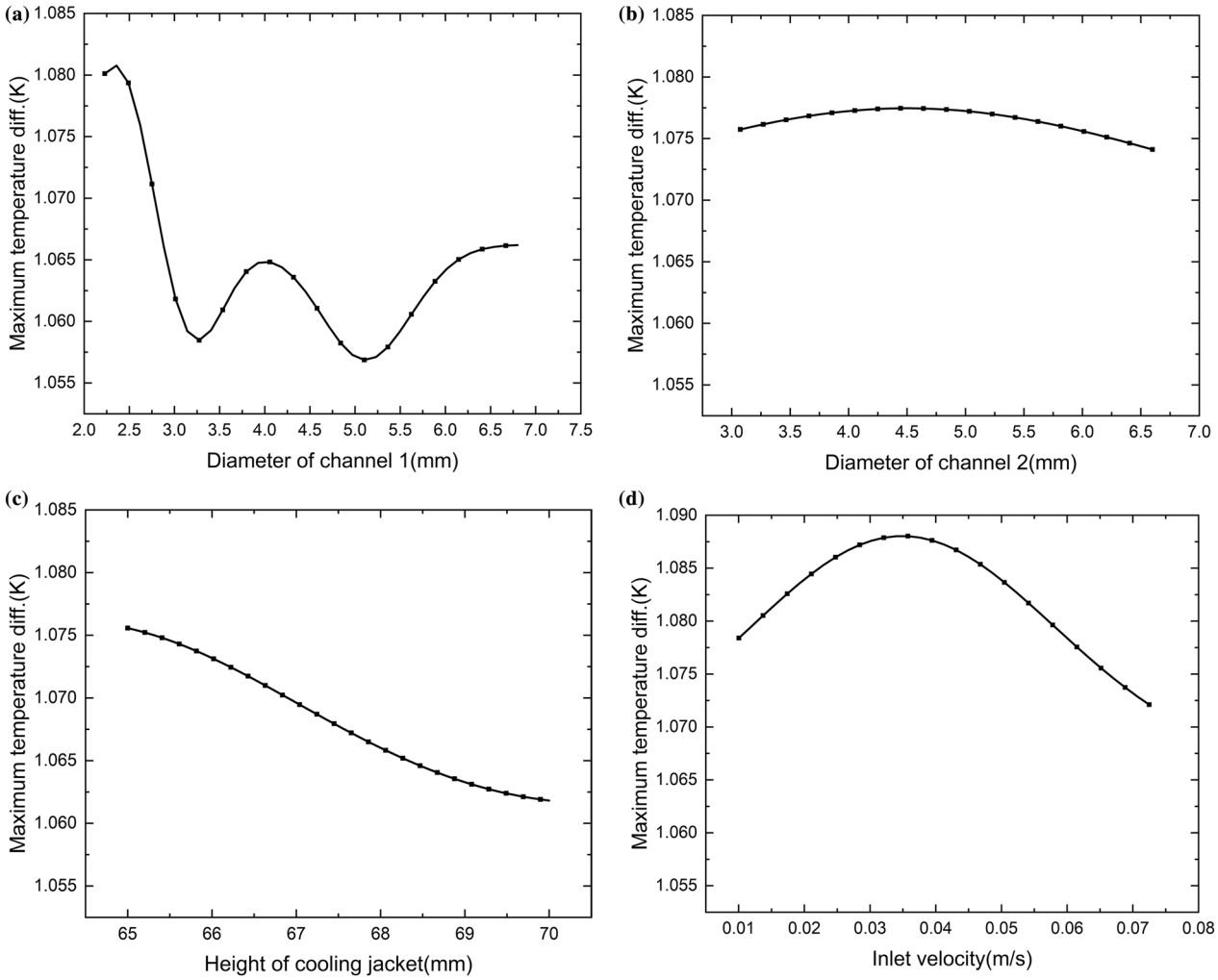

Figure 18 The prediction of the maximum temperature difference of the BTM system (first-order terms)

rate, the optimized average core temperature battery is 306.44 K. Compared with the original design, the maximum temperature difference remains within an acceptable range.

6 Conclusions

This paper developed a new BTM system based on liquid cooling to enhance heat transfer in the battery packs. The Kriging method is adopted to establish an approximate heat transfer model in the BTM system. In this approximate model, four sensitive factors affect the average temperature of the battery core and the maximum temperature difference. Besides, the MOPSO method is also used to optimize the design of the BTM system, and the optimal performance condition is obtained under 4 C discharge rate. The following concluding remarks can be drawn.

(1) The new battery pack BTM system can obtain a more uniform temperature distribution by adjusting the cooling channels in the staggered flow direction.
(2) The approximate model of the Kriging method significantly reduces the cost of computational resources and provides high accuracy.
(3) Compared with the original BTM system, the optimized BTM system can enhance heat transfer and obtain a more uniform temperature distribution.

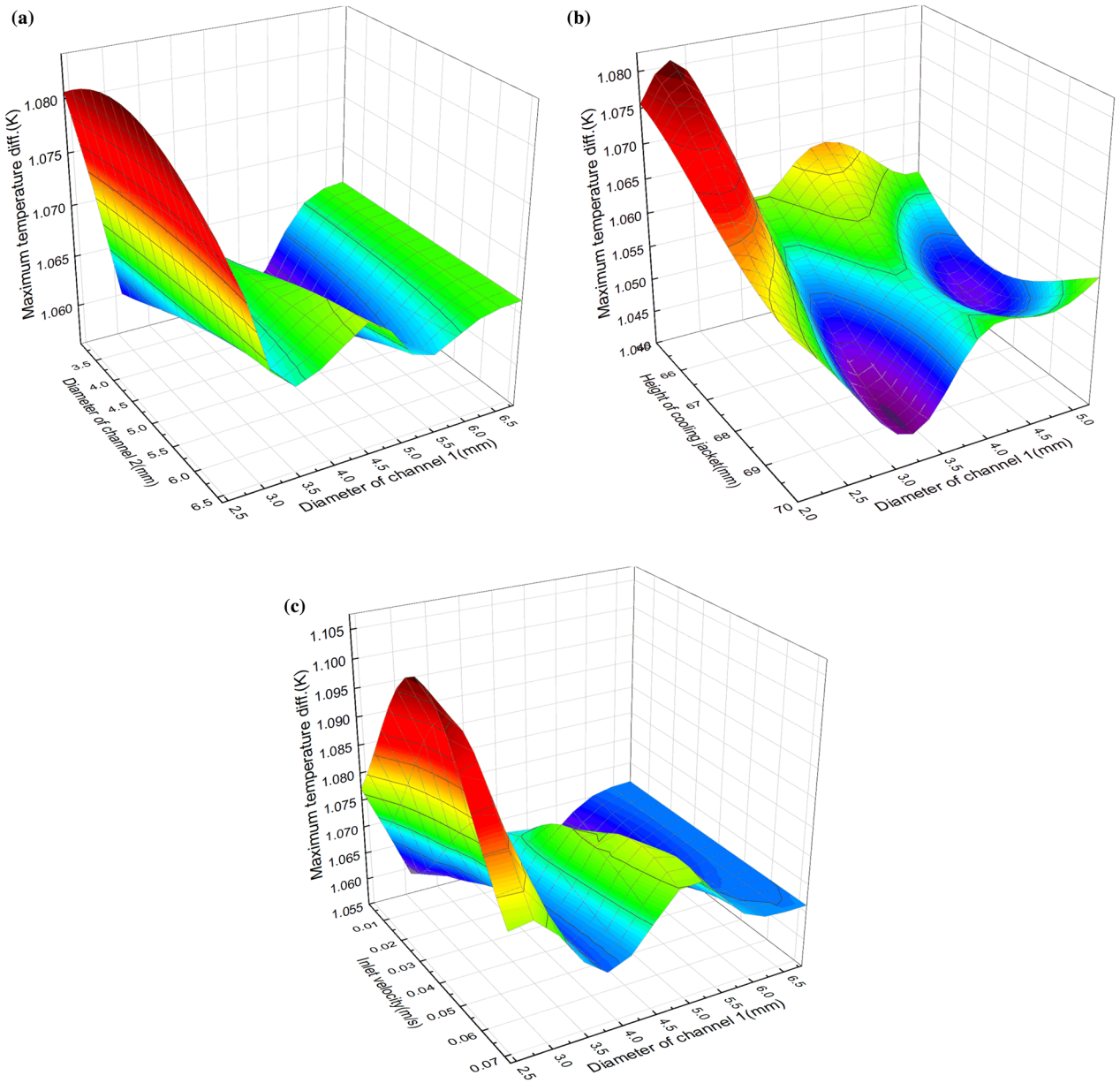

Figure 19 The prediction of the maximum temperature difference of BTM system (second-order terms)

Table 4 Original parameters and optimized parameter values

	Design variables	Original design	Optimized design
Input parameters	d_1 (mm)	1.5	4.3
	d_2 (mm)	2.0	4.9
	h (mm)	68.00	68.19
	v_0 (m/s)	0.005	0.045265
Output parameters	Average core temperature (K)	307.03	306.44
	Maximum temperature difference (K)	1.03	1.0605

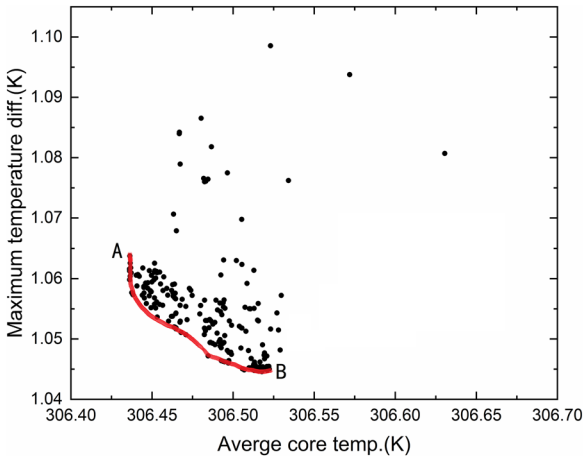

Figure 20 Pareto solution set of average core temperature and maximum temperature difference

Meanwhile, the risk of thermal runaway propagation is reduced.

Acknowledgements
Not applicable.

Author contributions
YS was in charge of the whole trial; YS wrote the manuscript; RB assisted with sampling and laboratory analyses; JM revised the manuscript. All authors read and approved the final manuscript.

Authors' Information
Yasong Sun, born in 1986, is currently an associate professor at School of Power and Energy, Northwestern Polytechnical University, China. He received his PhD degree from Northwestern University, China, in 2011. His research interests include heat transfer in power battery.
Rui-Huai Bai, born in 1997, is currently a master candidate at School of Power and Energy, Northwestern Polytechnical University, China.
Jing Ma, born in 1986, is currently an associate professor at School of Automobile, Chang'an University, China. She received her joint PhD degree from University of Texas at Austin, USA and Northwestern University, China, in 2014.

Funding
Supported by National Natural Science Foundation of China (Grant Nos. 51976173, 51976014), Jiangsu Provincial Natural Science Foundation of China (Grant No. BK20201204), and Basic Research Program of Taicang (Grant No. TC2019JC01).

Competing Interests
The authors declare no competing financial interests.

Author Details
[1]School of Power and Energy, Northwestern Polytechnical University, Xi'an 710072, China. [2]Center of Computational Physics and Energy Science, Yangtze River Delta Research Institute of NPU, Northwestern Polytechnical University, Taicang 215400, China. [3]School of Automobile, Chang'an University, Xi'an 710064, China.

Received: 28 October 2021 Revised: 20 May 2022 Accepted: 14 June 2022
Published online: 30 July 2022

References

[1] T Bandhauer, S Garimella, T F Fuller. A critical review of thermal issues in lithium-ion batteries. *Journal of the Electrochemical Society*, 2011, 158(3): R1.
[2] L Sheng, L Su, H Zhang, et al. Numerical investigation on a lithium-ion battery thermal management utilizing a serpentine-channel liquid cooling plate exchanger. *International Journal of Heat and Mass Transfer*, 2019, 141: 658-668.
[3] Q Wang, B Jiang, B Li, et al. A critical review of thermal management models and solutions of lithium-ion batteries for the development of pure electric vehicles. *Renewable and Sustainable Energy Reviews*, 2016, 64: 106-128.
[4] J Q E, Y Meng, J W Chen, et al. Effects of the different air-cooling strategies on cooling performance of a lithium-ion battery module with baffle. *Applied Thermal Engineering*, 2018, 144: 231-241.
[5] S Landini, J Leworthy, TS O'Donovan. A review of phase change materials for the thermal management and isothermalisation of lithium-ion Cells. *Journal of Energy Storage*, 2019, 25: 10087.
[6] H Yang, H Zhang, S Yang, et al. Numerical analysis and experimental visualization of phase change material melting process for thermal management of cylindrical power battery. *Applied Thermal Engineering*, 2018, 128: 489-499.
[7] J Le, H Y Zhang, J W Li, et al. Thermal performance of a cylindrical battery module impregnated with PCM composite based on thermoelectric cooling. *Energy*, 2019, 188: 116048.
[8] J Chen, S Kang, J Q E, et al. Effects of different phase change material thermal management strategies on the cooling performance of the power lithium-ion batteries: A review. *Journal of Power Sources*, 2019, 442: 227228.
[9] J Q E, Y Zeng, Y Jin, et al. Heat dissipation investigation of the power lithium-ion battery module based on orthogonal experiment design and fuzzy grey relation analysis. *Energy*, 2020, 211: 118596.
[10] X H Zhao, E Jiaqiang, G Wu, et al. A review of studies using graphenes in energy conversion, energy storage and heat transfer development. *Energy Conversion and Management*, 2019, 184: 581-599.
[11] S Kohn, G Berdichevsky, B Hewett. Tunable frangible battery pack system. US Patent No. 7.923.144, April 12, 2011.
[12] J T Zhao, Z H Rao, Y M Li. Thermal performance of mini-channel liquid cooled cylinder-based battery thermal management for cylindrical lithium-ion power battery. *Energy Conversion and Management*, 2015, 103: 157-165.
[13] Z H Rao, Z Qian, Y Kuang, et al. Thermal performance of liquid cooling based thermal management system for cylindrical lithium-ion battery module with variable contact surface. *Applied Thermal Engineering*, 2017, 123: 1514-1522.
[14] L Sheng, H Y Zhang, L Su, et al. Effect analysis on thermal profile management of a cylindrical lithium-ion battery utilizing a cellular liquid cooling jacket. *Energy*, 2021, 220: 119725.
[15] P R Tete, M M Gupta, S S Joshi, et al. Numerical investigation on thermal characteristics of a liquid-cooled lithium-ion battery pack with cylindrical cell casings and a square duct. *Journal of Energy Storage*, 2022, 48: 104041.
[16] Z Deng, X Hu, X Lin, et al. A reduced-order electrochemical model for all-solid-state batteries. *IEEE Transactions on Transportation Electrification*, 2021, 7(2): 464–473.
[17] S A Hallaj, H Maleki, J S Hong, et al. Thermal modeling and design considerations of lithium-ion batteries. *Journal of Power Sources*, 1999, 83: 1-8.
[18] M Al-Zareer, I Dincer, M A Rosen. A review of novel thermal management systems for batteries. *International Journal of Energy Research*, 2018, 42: 3182-3205.
[19] Z H Rao, Q C Wang, C L Huang. Investigation of the thermal performance of phase change material/mini-channel coupled battery thermal management system. *Applied Energy*, 2016, 164: 659-669.
[20] COMSOL Multiphysics. Introduction to COMSOL Multiphysics. COMSOL Multiphysics, Burlington, MA, February 9, 2018.
[21] M Doyle, J Newman, A S Gozdz, et al. Comparison of modeling predictions with experimental data from plastic lithium-ion cells. *Journal of the Electrochemical Society*, 1996, 143(6): 1890.
[22] B Koo, P Goli, A V Sumant, et al. Toward lithium-ion batteries with enhanced thermal conductivity. *ACS Nano*, 2014, 8(7): 7202-7207.

[23] M Doyle, T F Fuller, J Newman. Modeling of galvanostatic charge and discharge of the lithium/polymer/insertion cell. *Journal of the Electrochemical Society*, 1993, 140(6): 1526.
[24] T F Fuller, M Doyle, J Newman. Simulation and optimization of the dual lithium-ion insertion cell. *Journal of the Electrochemical Society*, 1994, 141(1): 1.
[25] M Al-Zareer, I Dincer, M Rosen. Development and evaluation of a new ammonia boiling based battery thermal management system. *Electrochim Acta*, 2018, 280: 340-352.
[26] K K Alireza, H Mohammadi. Multi-objective optimization in pavement management system using NSGA-II method. *Journal of Transportation Engineering, Part B: Pavements*, 2018, 144(2): 04018016.
[27] S Ramesh, S Kannan, S Baskar. Application of modified NSGA-II algorithm to multi-objective reactive power planning. *Applied Soft Computing*, 2012, 12(2): 741-753.
[28] I Kaymaz. Application of kriging method to structural reliability problems. *Structural Safety*, 2005, 27(2): 133-151.